RESEARCH ARTICLE

PLANT SCIENCE

Molecular insights into the complex mechanics of plant epidermal cell walls

Yao Zhang[1], Jingyi Yu[1], Xuan Wang[1], Daniel M. Durachko[1], Sulin Zhang[2]*, Daniel J. Cosgrove[1]*

Plants have evolved complex nanofibril-based cell walls to meet diverse biological and physical constraints. How strength and extensibility emerge from the nanoscale-to-mesoscale organization of growing cell walls has long been unresolved. We sought to clarify the mechanical roles of cellulose and matrix polysaccharides by developing a coarse-grained model based on polymer physics that recapitulates aspects of assembly and tensile mechanics of epidermal cell walls. Simple noncovalent binding interactions in the model generate bundled cellulose networks resembling that of primary cell walls and possessing stress-dependent elasticity, stiffening, and plasticity beyond a yield threshold. Plasticity originates from fibril-fibril sliding in aligned cellulose networks. This physical model provides quantitative insight into fundamental questions of plant mechanobiology and reveals design principles of biomaterials that combine stiffness with yielding and extensibility.

The primary cell wall physically controls many key features of growing plant cells, including size, shape, growth, water/turgor relations, mechanical strength, and defense against pathogens (*1*). Comprising three distinctive polysaccharides (cellulose, hemicelluloses, and pectins), the wall is often organized as a multilayer nanostructure, particularly conspicuous in epidermal walls that physically protect and limit growth of leaves and stems (*2*, *3*). Within individual layers (lamellae), stiff cellulose fibrils (~3 nm wide, traditionally called microfibrils) form a reticulated, noncovalent network aligned in a common direction that varies among lamellae, while hemicelluloses bind noncovalently to cellulose and well-hydrated pectins form a gel-like matrix hosting the stiff cellulose network. This cross-lamellate architecture contrasts with the network structures of soft and highly stretchable animal skins (*4*), brick-and-mortar structures in tough nacres (*5*), Bouligand (helicoidal) structures in impact-resistant cuticles of crustaceans (*6*), and many fiber-based biogels (*7*). Studies of such biomaterials have revealed how microstructures contribute to macroscale material properties (*7*–*9*), but this level of structure-function understanding has not yet been achieved for plant primary cell walls. An understanding of force distribution, microfibril movements, and reshaping of wall structure in response to mechanical forces can provide molecular insights into the mechanobiology of plant growth (*10*–*12*), responses to environmental and biotic stresses (*13*), and engineering of multifunctional materials (*14*, *15*).

Tensile tests of growing cell walls typically distinguish reversible (elastic) and irreversible (plastic) deformations (*16*–*18*). These empirical measurements lack a quantitative framework to connect macroscale mechanics to microscale responses. The development of this framework has been hindered by uncertainties of wall structure and by the difficulties of mechanical modeling of complex organs with heterogeneous cell walls. Here, we focused on the outer epidermal wall of onion scale as a primary cell wall with key advantages (*19*). It can be isolated as centimeter-wide peels that are large and strong enough for mechanical testing, yet are only one cell wall thick (~7 μm), offering a simplified material for structural and mechanical analyses (fig. S1). Imaging by atomic force microscopy (AFM) revealed its cross-lamellate organization and documented complex nanoscale motions of cellulose microfibrils during stretching and enzymatic loosening (*19*–*21*).

To bridge the gap between macroscale mechanical behaviors and microscale microfibril motions, we turned to mesoscale coarse-grained molecular dynamics (CGMD) simulations. In contrast to continuum and finite-element models of cell walls (which generally lack dynamic polymer behaviors) and atomistic simulations (which cannot capture wall mechanical behaviors because of length-scale limitations), CGMD simulations encompass molecular-scale behaviors with computational efficiency (*22*). Because CGMD models lump multiple atomic interactions between molecules, they can simulate wall-stretching experiments (*23*), thereby offering multiscale insights into wall mechanics. We combined this modeling approach with tensile testing of epidermal walls to generate insights into the microstructural bases for the complex nonlinear response of primary cell walls to tensile force. The model simulated aspects of wall assembly, uncovered the physical basis for wall plasticity, and revealed the uneven distribution of tensile stresses within epidermal walls; these stresses have been hypothesized to modulate cytoskeletal dynamics and morphogenesis (*10*–*12*).

Design and assembly of the model wall

Our model is based on the cross-lamellate onion epidermal wall (Fig. 1A) (*19*–*21*). Cellulose microfibrils and matrix polysaccharides (xyloglucan, the main hemicellulose, and homogalacturonan, the dominant pectin) were represented by chains of beads tuned to best estimates of their corresponding physical properties (*24*). Homo-bead interaction potentials were set to match the axial and bending stiffnesses of the corresponding polysaccharides (table S1), whereas interbead interaction potentials captured the noncovalent binding interactions between polysaccharides based on atomistic simulations (table S2) (*24*, *25*). The full simulation consisted of four lamellae with initial dimensions of 900 nm × 900 nm × 160 nm and with varied cellulose orientations (Fig. 1). Wall composition matched that of the onion epidermal wall (*24*).

To generate a wall-like structure, we initially placed cellulose microfibrils into a common orientation midplane of each lamella (Fig. 1B), mimicking surface deposition by synthase complexes (*26*) under cellular guidance (*27*). Cellulose orientations varied among lamellae. Xyloglucan and pectin chains were randomly dispersed in the simulation domain, roughly mimicking the result of exocytosis of matrix polysaccharides. The system was dynamically equilibrated, allowing spontaneous movements and interactions of all polymers. Cellulose microfibrils within lamellae self-assembled into coherent two-dimensional networks resembling, to a first approximation, the bundled cellulose organization observed by AFM (*20*) (compare Fig. 1, A and C). In further simulations, microfibril crossover as observed by AFM was mimicked by dispersing 20% of the microfibrils within each lamella at a divergent angle (Fig. 1, D to K, and fig. S2). After equilibration, xyloglucans adhered to cellulose microfibrils as extended chains and random coils (Fig. 1, F to K), resembling actual xyloglucan chains observed in onion walls (*28*). Pectins were distributed throughout the space and made extensive but weak contacts with cellulose surfaces, consistent with results from solid-state nuclear magnetic resonance (*29*), AFM (*19*, *20*), and binding studies. Cellulose networks in the four lamellae remained physically distinct (Fig. 1G). These equilibration results—based on minimal assumptions of the physical properties, deposition patterns, and interactions of wall polymers—demonstrate that

---

[1]Department of Biology, Pennsylvania State University, University Park, PA 16802, USA. [2]Department of Engineering Science and Mechanics and Department of Biomedical Engineering, Pennsylvania State University, University Park, PA 16802, USA.
*Corresponding author. Email: suz10@psu.edu (S.Z.); dcosgrove@psu.edu (D.J.C.)

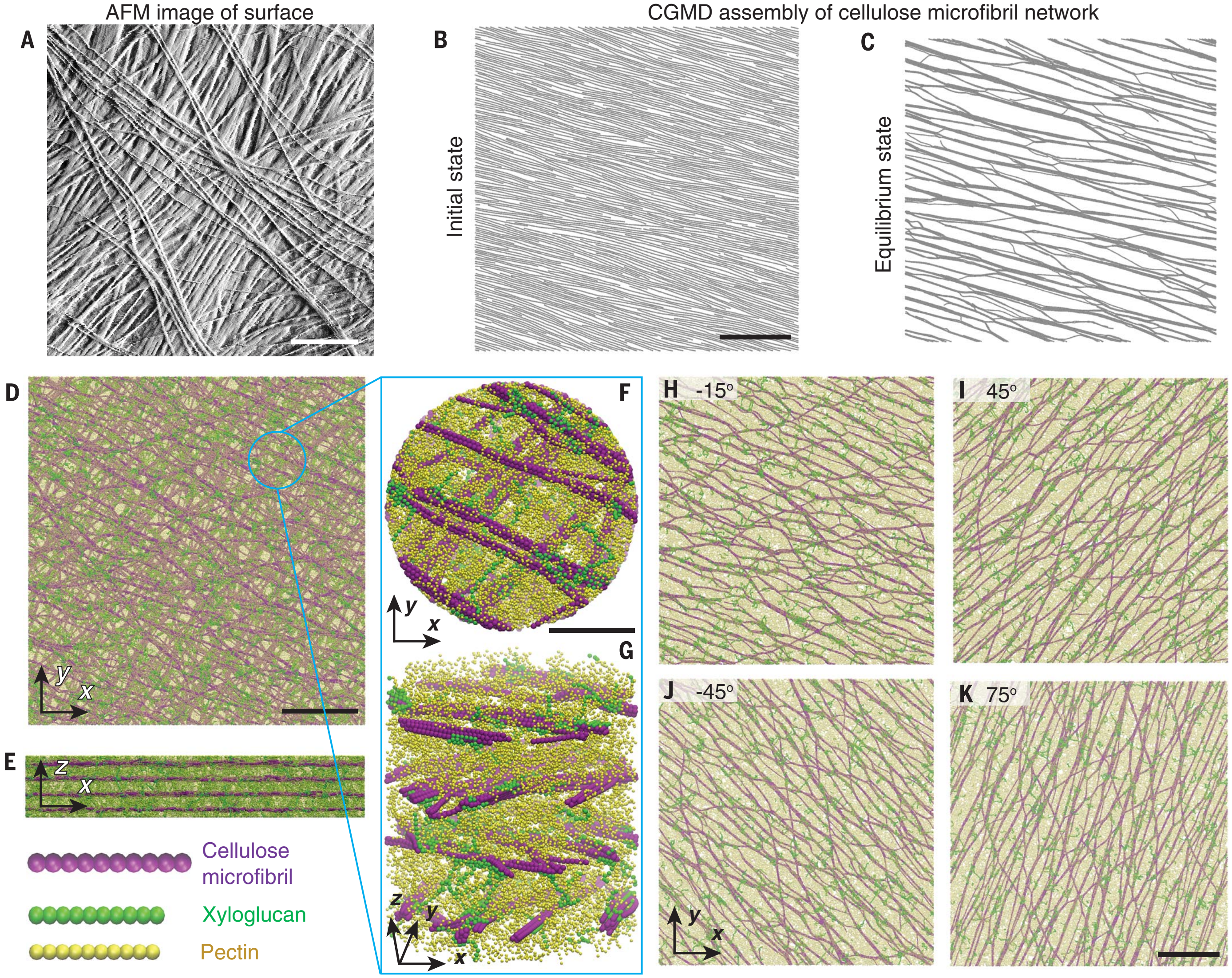

Fig. 1. Assembly of the CGMD model of a plant primary cell wall. (**A**) AFM image of newly deposited surface of outer epidermal wall of onion scale, showing the cross-lamellate organization of cellulose microfibrils [peak force error map, 1 × 1 μm; after (*20*)]. (**B** and **C**) Microfibril orientation in a single-lamella model before energy equilibration (B) and after (C), shown at the same scale. (**D** and **E**) Top (D) and side (E) views of the four-lamella wall after equilibration, shown at the same scale. (**F** and **G**) Close-ups of top and side views. (**H** to **K**) Top views of the four lamellae with varying initial cellulose orientation, shown at the same scale. Scale bars, 200 nm [(A) to (E) and (H) to (K)], 25 nm [(F) and (G)].

macromolecular morphologies resembling that of the actual wall can emerge from the collective physical interactions incorporated in the model.

Influence of cellulose on nonlinear mechanics

We used the model with four lamellae to represent the polylamellate epidermal wall and to compare its tensile responses to those of the actual wall. Cellulose orientations of the lamellae (−15°, +45°, −45°, +75°) were chosen to represent the range of cellulose angles while approximating a net isotropic structure (*30*). The structure was stretched uniaxially under constant-volume conditions; Fig. 2A shows the stress-strain result. The slope (modulus) was highly nonlinear (Fig. 2B): initially constant to ~1% strain, followed by a curvilinear region of increasing stiffness (increasing slope) to ~8% strain, and then a region of decreasing slope. As detailed below, the decrease in slope results from plastic yielding of selective wall components. The model's stress-strain behaviors closely recapitulated that of real epidermal walls (Fig. 2, A and B, and fig. S2) (*18*, *19*). These plots are characteristic of primary cell walls and are commonly used to assess wall extensibilities (*16*–*18*), although without microstructural insights.

Decomposition of wall stress into its components (Fig. 2C) (*24*) revealed that cellulose microfibrils carried most of the stress, despite the abundance of pectin and despite the frequent bridging of xyloglucans between microfibrils. This result is consistent with experimental observations that xyloglucanase and pectolyase digestions negligibly affect the tensile stiffness of onion epidermal walls (*21*). Increasing the binding energies between cellulose and matrix polysaccharides negligibly altered wall stiffness (Fig. 2E and fig. S5), whereas tuning of cellulose-cellulose interactions modulated stiffness at strains greater than 6% (Fig. 2F). Strengthening cellulose-cellulose interactions substantially reduced plasticity, manifested here as a declining stress-strain slope above 6% strain, delaying its onset to higher stresses. Additional simulations showed that xyloglucan length, pectin length, and pectin cross-linking had little effect on tensile responses, whereas the length, density,

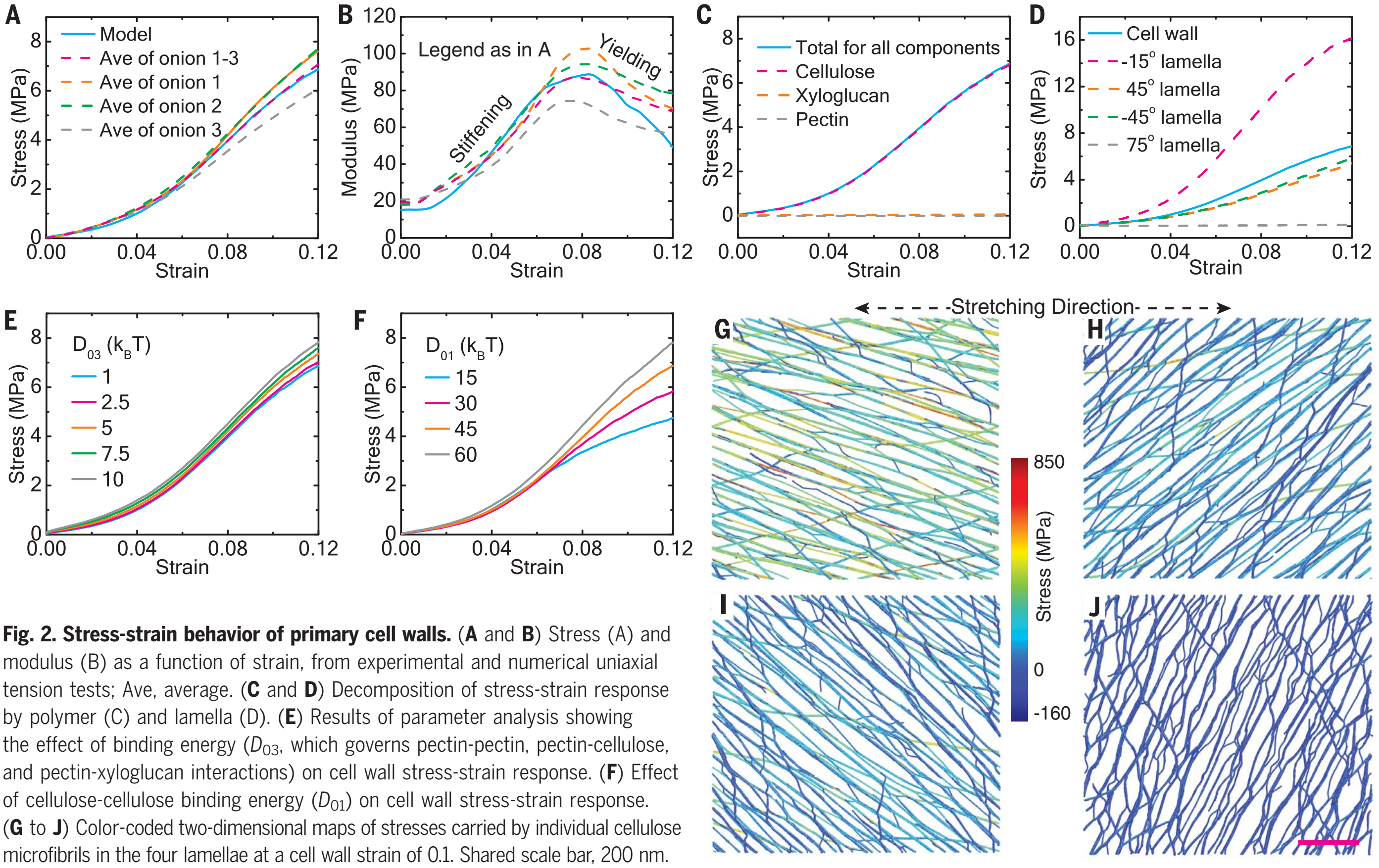

Fig. 2. Stress-strain behavior of primary cell walls. (**A** and **B**) Stress (A) and modulus (B) as a function of strain, from experimental and numerical uniaxial tension tests; Ave, average. (**C** and **D**) Decomposition of stress-strain response by polymer (C) and lamella (D). (**E**) Results of parameter analysis showing the effect of binding energy (D_{03}, which governs pectin-pectin, pectin-cellulose, and pectin-xyloglucan interactions) on cell wall stress-strain response. (**F**) Effect of cellulose-cellulose binding energy (D_{01}) on cell wall stress-strain response. (**G** to **J**) Color-coded two-dimensional maps of stresses carried by individual cellulose microfibrils in the four lamellae at a cell wall strain of 0.1. Shared scale bar, 200 nm.

and distribution of cellulose microfibrils had substantial effects (fig. S5). Thus, cellulose-cellulose interactions dominate the mechanical behaviors of this wall model, consistent with experimental results (*16*, *21*).

The dominance of cellulose results from its high axial stiffness, low bending stiffness, and strong lateral bonding. Together these properties enable cellulose microfibrils to aggregate extensively into laterally bonded bundles, forming strong, highly anisotropic planar networks that directly transmit tensile forces between microfibrils. In contrast, the entropic flexibility of matrix polysaccharides resulted in lower polymer stiffness (fig. S6), less stable networks, and smaller contributions to tensile mechanics.

Stress was greatest in the lamella (–15°) aligned most closely to the stretching direction, whereas the 75° lamella carried negligible stress (Fig. 2D). Lamellae with intermediate orientations developed small stresses at higher strains. The –15° lamella stiffened at low strains, whereas at high strains its stress-strain slope flattened as a result of microfibril sliding (see below). In contrast, the ±45° lamellae remained in the stiffening regime throughout the stretching process.

Stress responses were further analyzed by color-coded maps of microfibrillar stresses at 10% wall strain (Fig. 2, G to J). Stresses were heterogeneous, with the greatest variability in the –15° lamella, which also displayed the largest total stress and the largest yielding at high strains. Because the real wall consists of many lamellae of different cellulose orientations, collectively it appears approximately isotropic in-plane (*30*), yet individual lamellae are highly anisotropic and are predicted to bear very different stresses upon uniaxial stretch.

Microfibril movements during wall stretching

In simulations of single lamellae with varied cellulose orientations, we observed five distinctive cellulose microfibril movements: (i) straightening, where end-to-end length increased with stretching (Fig. 3A); (ii) curving, where end-to-end length decreased (Fig. 3B); (iii) sliding, where aligned microfibrils slipped past each other (Fig. 3C); (iv) angular reorientation, where microfibril direction changed (Fig. 3D); and (v) changes in bundling, where microfibrils altered their lateral associations (fig. S7 and movies S1 and S2). These movements replicated those detected in AFM analyses of stretching epidermal walls (*19*).

Changes in microfibril conformation were analyzed by plotting the average end-to-end length (L_E) as a function of strain (Fig. 3E). In lamellae with large orientation angles (60° and 90°), microfibrils became more curved as a result of wall compression transverse to the stretching direction. In lamellae with small and intermediate microfibril angles (0°, 30°, and 45°), microfibrils straightened, but this action ceased at a critical strain when microfibril sliding began (the transition from solid to dashed lines in Fig. 3E). This straightening-to-sliding transition point marks the yield threshold.

Cellulose reorientation was quantified as the change of the average orientation angle (Δβ) during stretching (*24*). As expected from geometry, lamellae with intermediate microfibril angles (30° to 60°) experienced larger reorientations than those oriented close to 0° or 90° (Fig. 3F). Collective reorientation was associated with increased microfibril bundling at large strains as microfibrils were drawn into closer proximity (movie S2). For microfibrils at 90°, stretching caused microfibril curving but no net angular change.

Figure 3G shows stress-strain curves annotated to indicate the major modes of microfibril movements during stretching. Microfibril straightening occurred during lamellar stiffening (increasing slope), whereas microfibril sliding became dominant at the later stage of decreasing slope (yielding). The straightening-to-sliding transition occurred at a larger critical strain in lamellae with larger initial orientation angle, but at a similar stress threshold.

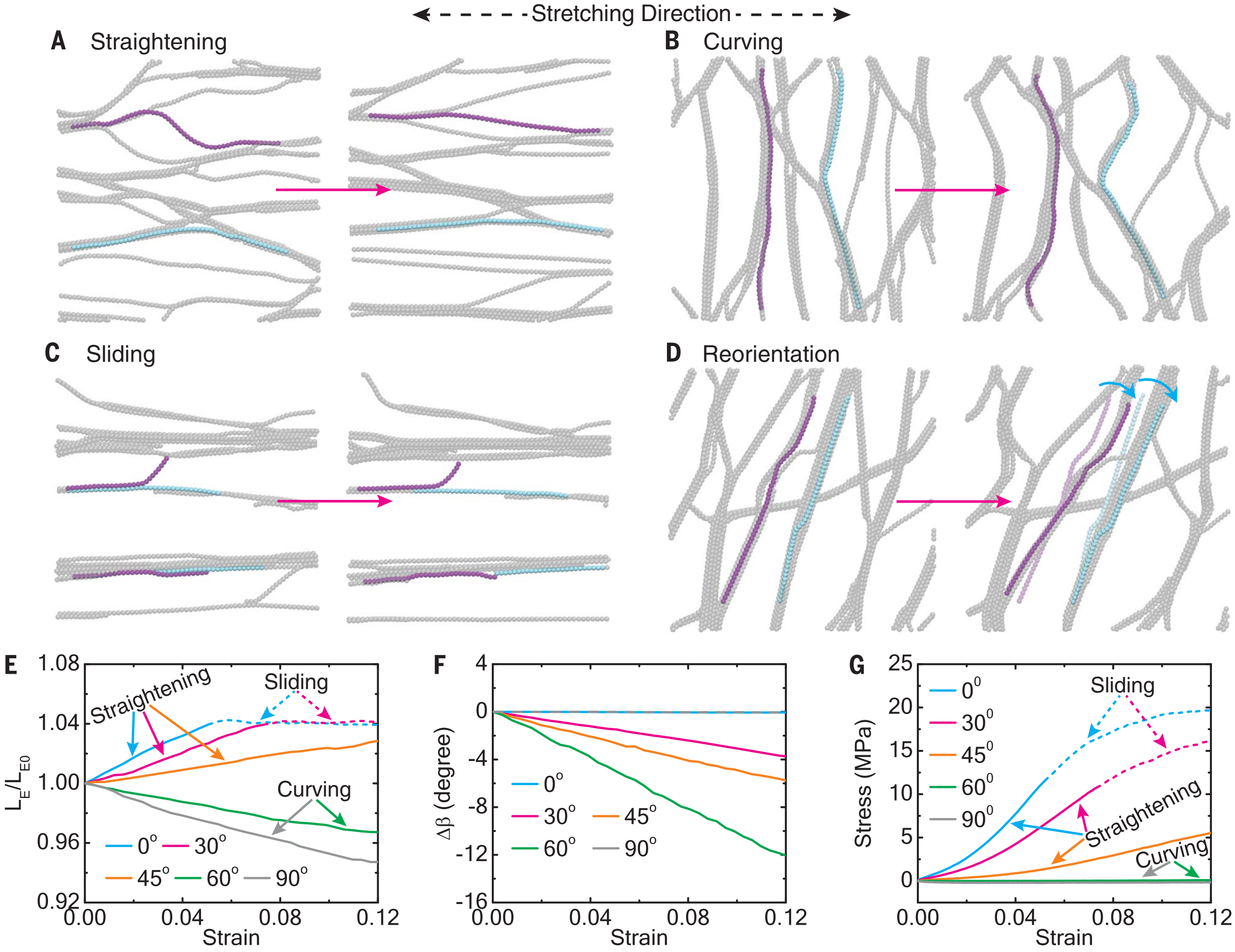

Fig. 3. Distinctive movements of cellulose microfibrils during uniaxial stretching of single lamellae. (**A** to **D**) Examples of microfibril movements (highlighted snapshots before and after movement), illustrating straightening (A), curving (B), sliding (C), and angular reorientation (D). (**E**) Normalized average end-to-end length of cellulose microfibrils, L_E/L_{E0}, as a function of wall strain for lamellae with different cellulose orientations. (**F**) Change in average orientation angle Δβ of cellulose microfibrils as a function of wall strain for lamellae with different cellulose orientations. (**G**) Wall stress as a function of strain for single-lamella wall model with various cellulose orientations, annotated to indicate the major modes of cellulose movement.

Energy dissipation and plasticity

We next investigated energy dissipation by stretching the walls (real and simulated) to the same stress value twice cyclically and measuring the loading and unloading stress-strain curves in both cycles. For real epidermal walls (Fig. 4A and fig. S8), loading and unloading curves in the first cycle followed different paths, revealing a large hysteresis and unrecoverable (plastic) deformation. Hysteresis indicates energy dissipation, represented by the area between the loading and unloading curves. Hysteresis is common in polymeric hydrogels, although its molecular basis varies in different materials (*31*, *32*). For the epidermal wall, the initial slope of the unloading curve was very steep, 290 MPa in this example, indicating high elastic stiffness despite the onset of plasticity.

The second loading curve followed a different path from the first, whereas the second unloading curve was nearly identical to the first. Subsequent cycles closely resembled the second cycle, indicating reversibility. This behavior contrasts with the progressive softening observed in animal tissues upon repeated stretching (*33*). From these results we distinguish two types of hysteresis: The second (reversible) cycle displays elastic hysteresis, whereas the first cycle includes an irreversible component due to plasticity (*17*).

In the corresponding model, cyclic extensions displayed similar behavior, including hysteresis and unrecoverable deformation (Fig. 4B). To elucidate the mechanisms underlying irreversible strain in the first cycle, we followed the evolution of L_E (straightening) of cellulose microfibrils as well as their average orientation β during the loading-unloading cycles. Both L_E and β in the four lamellae showed small irreversible changes at the end of the first cycle (Fig. 4, C and D, magenta arrows). We estimate (*24*) that microfibril sliding made the largest contribution (~63%) to irreversible extension of the −15° lamella, with smaller contributions from permanent microfibril straightening (~25%) and angular reorientation (~11%). At larger strains, cellulose sliding may account for a larger fraction of irreversible deformation. In the absence of sliding during the second cycle, cellulose straightening, curving, and reorientation were fully reversible. These results demonstrate coupling of the four modes of cellulose restructuring as well as different microfibril motions during loading and unloading.

The difference in hysteresis between the first and second stretch cycles for the model clarifies the energy dissipation mechanisms involved in wall stretching. In the first cycle, cellulose-cellulose sliding coupled to other conformational changes underlies irreversible deformation. Energy dissipation is largest in lamellae with cellulose aligned in the stretching direction (fig. S9), where fibril sliding is

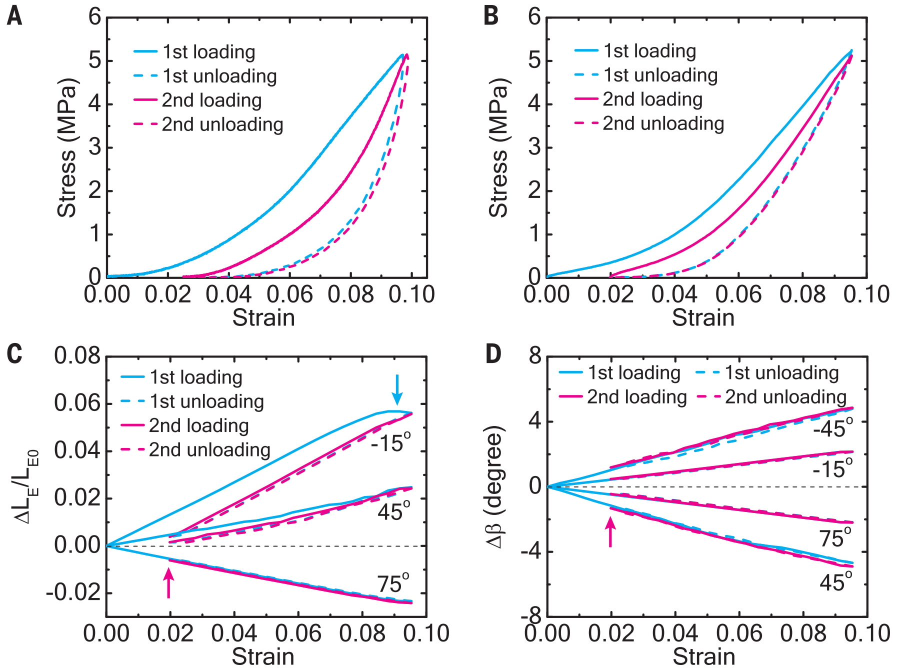

Fig. 4. Cell wall stress-strain responses during cyclic loading and unloading. (**A**) Experimental stress-strain response of onion epidermal strip (representative result of five trials). (**B**) Modeled numerical stress-strain response to strain matching the experimental data in (A) during cyclic loading and unloading. (**C**) Change in normalized average end-to-end length ($\Delta L_E/L_{E0}$) of cellulose microfibrils as a function of strain. The cyan arrow indicates the region where L_E reaches a plateau and sliding occurs in the −15° lamella. (**D**) Change in average orientation angle (β) of cellulose microfibrils as a function of strain. The magenta arrows in (C) and (D) indicate the unrecovered L_E and β, respectively, after the first stretch.

greatest. The second cycle exhibits only reversible hysteresis, likely arising from breaking and reforming noncovalent bonds between polysaccharides during loading and unloading (movie S2).

Calculations of cellulose bond lengths during the initial phase of unloading predict substantial elastic contraction of cellulose microfibrils aligned in the stretch direction, accounting for 80% of the initial wall contraction (fig. S9). This finding contrasts with a common view that cellulose is nearly inextensible in primary cell walls, but it is consistent with the steep slope of unloading (Fig. 4A) and the high axial stiffness of cellulose microfibrils (*14*, *15*, *34*).

Perspectives and outlook

Our physical model successfully assembled polysaccharides into a structure with supramolecular morphology and complex tensile behaviors resembling those of actual epidermal walls. The model shows how these traits, common to primary cell walls, may emerge from the collective elementary physical interactions between wall polysaccharides. Previous atomistic models simulated component interactions [e.g., xyloglucan binding to cellulose surfaces (*35*)], but this approach cannot reach the length scale needed to investigate the origins of wall mechanics or cellulose networks. In larger-scale finite-element wall models (*36*, *37*), cellulose was represented as stiff rods cross-linked at fixed points by thinner and stretchier rods, representing xyloglucan. In yet other studies (*38*, *39*), wall growth was modeled by continuum equations simulating insertion of pectins into the wall. Absent from these models are molecular processes central to our findings, including bundling and sliding of cellulose microfibrils, entropic effects on polymer conformations, and dynamic matrix-cellulose interactions. These realistic polysaccharide behaviors are enabled by the GCMD approach. What emerges from these interactions is a dynamic load-bearing network in which tensile forces are transmitted primarily through direct lateral contacts between microfibrils, rather than by matrix polysaccharides.

The CGMD simulations offer insights into the molecular bases of wall elasticity, plasticity above a yield threshold, stiffening at small strains, reduction in modulus at high strains, and energy dissipation during stretching. They clarify the mechanical contributions made by the three major wall polysaccharides, showing that complex cellulose movements dominate tensile mechanics. The results also offer a rationale for why enzymatic digestion of xyloglucan and pectin produced little effect on tensile stiffness or plasticity (*16*, *21*), contrary to expectations based on conventional tethered-network models of cell wall organization (*1*, *40*). With fewer lamellae than the actual wall and with polysaccharides simplified to CGMD representations, the model's behavior may differ from the actual wall in fine detail (e.g., in hysteresis and the exact shape of the loading and unloading curves). Moreover, the actions of expansins and other wall-modifying proteins (*1*) are not part of this model.

In a broader biological context, matrix polysaccharides likely influence tensile mechanics by modulating how cellulose microfibrils assemble into networks and by limiting the action of cellulose-modifying proteins. Microtubule dynamics and other cellular processes (*10*, *11*, *27*, *41*, *42*) ultimately influence wall mechanics by controlling patterns of cellulose microfibril deposition and the resulting network structure. These represent additional cellular mechanisms that control wall mechanics at a hierarchical level beyond the physical treatment presented here.

The highly nonlinear stress-strain behavior of primary cell walls has long been used to estimate empirical wall extensibilities for growth studies (*16*–*18*). Our results give a clearer basis for interpreting the meaning of such extensibilities. Cellulose sliding seen here resembles "slip-stick" deformation of wet wood (*43*–*45*), which also retains considerable stiffness after plastic yielding. Woody walls substantially differ from primary cell walls in composition, organization, and material properties, and their plasticity has been ascribed to viscous shearing of hemicelluloses between microfibrils (*23*, *43*, *45*). Direct sliding between microfibrils, as modeled here, may also contribute to the plastic deformation of woody cell walls, and this should be a subject of future investigation.

Finally, numerous studies in plant mechanobiology have implicated cell wall stress as an informational factor modulating microtubule organization and plant cell morphogenesis [e.g., (*10*–*12*, *42*)]. By clarifying how wall stresses are transmitted at the microscale and distributed within the wall, our study provides a physical framework for mechanistic investigations of how wall stresses relate to microtubule organization. Our results also clarify the distinctions among wall stress, lamellar stress, and stress in cellulose microfibrils (which can be two orders of magnitude greater than wall stress). The ingenious microstructural and architectural design of plant epidermal cell walls suggests ways to engineer strong and extensible fibrous materials with multifunctional applications.

REFERENCES AND NOTES

1. D. J. Cosgrove, *Nat. Rev. Mol. Cell Biol.* **6**, 850–861 (2005).
2. M. Lipowczan, D. Borowska-Wykret, S. Natonik-Bialon, D. Kwiatkowska, *J. Exp. Bot.* **69**, 4349–4362 (2018).
3. D. J. Cosgrove, *Curr. Opin. Plant Biol.* **46**, 77–86 (2018).
4. M. Vatankhah-Varnosfaderani *et al.*, *Science* **359**, 1509–1513 (2018).
5. H. Gao, B. Ji, I. L. Jager, E. Arzt, P. Fratzl, *Proc. Natl. Acad. Sci. U.S.A.* **100**, 5597–5600 (2003).

6. J. C. Weaver *et al*., *Science* **336**, 1275–1280 (2012).
7. A. S. G. van Oosten *et al*., *Nature* **573**, 96–101 (2019).
8. M. A. Meyers, J. McKittrick, P. Y. Chen, *Science* **339**, 773–779 (2013).
9. F. Barthelat, Z. Yin, M. J. Buehler, *Nat. Rev. Mater.* **1**, 16007 (2016).
10. O. Hamant, D. Inoue, D. Bouchez, J. Dumais, E. Mjolsness, *Nat. Commun.* **10**, 2360 (2019).
11. A. Sampathkumar *et al*., *eLife* **3**, e01967 (2014).
12. S. Verger, Y. Long, A. Boudaoud, O. Hamant, *eLife* **7**, e34460 (2018).
13. K. Hu *et al*., *Nat. Plants* **3**, 17009 (2017).
14. C. Chen *et al*., *Nat. Rev. Mater.* **5**, 642–666 (2020).
15. J. Song *et al*., *Nature* **554**, 224–228 (2018).
16. Y. B. Park, D. J. Cosgrove, *Plant Physiol.* **158**, 1933–1943 (2012).
17. R. Cleland, *Planta* **74**, 197–209 (1967).
18. A. J. Bidhendi, H. Li, A. Geitmann, *Botany* **98**, 49–64 (2020).
19. T. Zhang, D. Vavylonis, D. M. Durachko, D. J. Cosgrove, *Nat. Plants* **3**, 17056 (2017).
20. T. Zhang, Y. Zheng, D. J. Cosgrove, *Plant J.* **85**, 179–192 (2016).
21. T. Zhang, H. Tang, D. Vavylonis, D. J. Cosgrove, *Plant J.* **100**, 1101–1117 (2019).
22. H. I. Ingólfsson *et al*., *Wiley Interdiscip. Rev. Comput. Mol. Sci.* **4**, 225–248 (2014).
23. D. C. Adler, M. J. Buehler, *Soft Matter* **9**, 7138–7144 (2013).
24. See supplementary materials.
25. Y. Zhang, E. P. DeBenedictis, S. Keten, *Soft Matter* **15**, 3807–3816 (2019).
26. P. Purushotham, R. Ho, J. Zimmer, *Science* **369**, 1089–1094 (2020).
27. J. Chan, E. Coen, *Curr. Biol.* **30**, 941–947.e2 (2020).
28. Y. Zheng, X. Wang, Y. Chen, E. Wagner, D. J. Cosgrove, *Plant J.* **93**, 211–226 (2018).
29. T. Wang, Y. B. Park, D. J. Cosgrove, M. Hong, *Plant Physiol.* **168**, 871–884 (2015).
30. K. Kafle *et al*., *Cellulose* **24**, 3145–3154 (2017).
31. X. Zhao, *Soft Matter* **10**, 672–687 (2014).
32. Z. Wang *et al*., *Proc. Natl. Acad. Sci. U.S.A.* **116**, 5967–5972 (2019).
33. K. M. Schmoller, A. R. Bausch, *Nat. Mater.* **12**, 278–281 (2013).
34. S. J. Eichhorn, *ACS Macro Lett.* **1**, 1237–1239 (2012).
35. Z. Zhao, V. H. Crespi, J. D. Kubicki, D. J. Cosgrove, L. H. Zhong, *Cellulose* **21**, 1025–1039 (2014).
36. H. Kha, S. C. Tuble, S. Kalyanasundaram, R. E. Williamson, *Plant Physiol.* **152**, 774–786 (2010).
37. R. Huang, A. A. Becker, I. A. Jones, *J. Eng. Math.* **95**, 121–154 (2015).
38. O. Ali, J. Traas, *Trends Plant Sci.* **21**, 398–409 (2016).
39. E. T. Smithers, J. Luo, R. J. Dyson, *J. Exp. Bot.* **70**, 3587–3600 (2019).
40. D. M. Cavalier *et al*., *Plant Cell* **20**, 1519–1537 (2008).
41. A. R. Paredez, C. R. Somerville, D. W. Ehrhardt, *Science* **312**, 1491–1495 (2006).
42. A. Sampathkumar, *Development* **147**, dev177964 (2020).
43. L. Köhler, T. Speck, H. C. Spatz, *Planta* **210**, 691–700 (2000).
44. L. H. Thomas *et al*., *Sci. Rep.* **11**, 453 (2021).
45. J. Keckes *et al*., *Nat. Mater.* **2**, 810–814 (2003).
46. LAMMPS data and code are at Zenodo, DOI 10.5281/zenodo.4543822.

ACKNOWLEDGMENTS

We thank E. Coen and L. Petridis for discussions and L. Wilson for technical assistance. **Funding:** This work was supported as part of the Center for Lignocellulose Structure and Formation, an Energy Frontier Research Center funded by the US Department of Energy, Office of Science, Basic Energy Sciences under award DE-SC0001090. **Author contributions:** Y.Z.: investigation, methodology, formal analysis, software, writing–original draft; J.Y.: investigation; X.W.: investigation; D.M.D.: investigation, methodology; S.Z.: methodology, supervision, writing–review and editing; D.J.C.: conceptualization, supervision, writing–review and editing, project administration, funding acquisition. **Competing interests:** The authors declare no competing interests. **Data and materials availability:** All data are available in the main text or the supplementary materials, and at (*46*).

SUPPLEMENTARY MATERIALS

science.sciencemag.org/content/372/6543/706/suppl/DC1
Materials and Methods
Figs. S1 to S9
Tables S1 and S2
Movies S1 and S2
References (*47*–*95*)
MDAR Reproducibility Checklist

15 October 2020; accepted 29 March 2021
10.1126/science.abf2824

Science

Molecular insights into the complex mechanics of plant epidermal cell walls

Yao Zhang, Jingyi Yu, Xuan Wang, Daniel M. Durachko, Sulin Zhang and Daniel J. Cosgrove

Science **372** (6543), 706-711.
DOI: 10.1126/science.abf2824

Computational analysis of cell walls

Layers of intertwined fibers make up plant cell walls. The various types of fibers respond differently to deformation. Cellulose microfibrils, for example, can stretch or curve, changing their end-to-end length, and can also slide past each other, reorient relative directions, and bundle with neighboring microfibrils. Zhang *et al.* developed a computational model based on observations of onion skin epidermis that describes how these complex changes in space govern cell wall mechanics. The results inform ways to engineer multifunctional fibrous materials.

Science, this issue p. 706

ARTICLE TOOLS	http://science.sciencemag.org/content/372/6543/706
SUPPLEMENTARY MATERIALS	http://science.sciencemag.org/content/suppl/2021/05/12/372.6543.706.DC1
REFERENCES	This article cites 95 articles, 14 of which you can access for free http://science.sciencemag.org/content/372/6543/706#BIBL
PERMISSIONS	http://www.sciencemag.org/help/reprints-and-permissions

Science (print ISSN 0036-8075; online ISSN 1095-9203) is published by the American Association for the Advancement of Science, 1200 New York Avenue NW, Washington, DC 20005. The title *Science* is a registered trademark of AAAS.